Regular Assembly of Polymer Nanoparticles by Optical Trapping Enhanced with a Random Array of Si Needles for Reconfigurable Photonic Crystals in Liquid

Regular Assembly of Polymer Nanoparticles by Optical Trapping Enhanced with a Random Array of Si Needles for Reconfigurable Photonic Crystals in Liquid

Itsuo Hanasaki, Tatsuya Shoji, and Yasuyuki Tsuboi

Hanasaki, I., Shoji, T., & Tsuboi, Y. (2019). Regular Assembly of Polymer Nanoparticles by Optical Trapping Enhanced with a Random Array of Si Needles for Reconfigurable Photonic Crystals in Liquid. *ACS Applied Nano Materials*, 2(12), 7637–7643. https://doi.org/10.1021/acsanm.9b01707

Regular Assembly of Polymer Nanoparticles by Optical Trapping Enhanced with Random Array of Si Needles for Reconfigurable Photonic Crystals in Liquid

Itsuo Hanasaki,*,† Tatsuya Shoji,‡ and Yasuyuki Tsuboi*,‡

† *Institute of Engineering, Tokyo University of Agriculture and Technology, Naka-cho 2-24-16, Koganei, Tokyo 184-8588, Japan*

‡ *Division of Molecular Materials Science, Graduate School of Science, Osaka City University, Sugimoto 3-3-138, Sumiyoshi, Osaka, 5558-8585, Japan*

E-mail: *hanasaki@cc.tuat.ac.jp; *twoboys@sci.osaka-cu.ac.jp

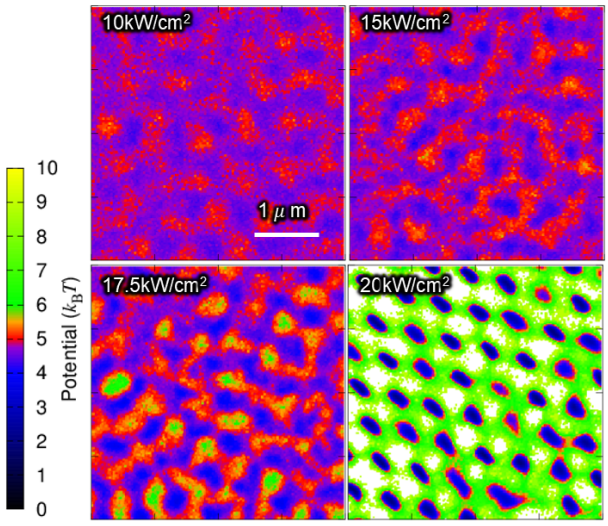

Abstract

We report the optical trapping of many particles with feasible laser powers by the nanostructured semiconductor-assisted (NASSCA) trapping technique. Furthermore, we have found that the random array of silicon needles with spacings substantially smaller than the nanoparticle sizes is advantageous not only for the trapping force field enhancement but also for the realization of close-packed assembly of nanoparticles. This counter-intuitive approach is promising for the realizations of collective structural orders such as reconfigurable photonic crystals in liquid, which have been often regarded to require either top-down templates or full self-assembly beyond control.

Keywords

Optical force, Optical trapping, Laser trapping, Particle assembly, Structural order, Colloidal crystal, Collective behavior, Particle tracking

Introduction

Optical trapping of single particles has a long history,[1] and the trapping force field enhancement by plasmonic optical tweezer (POT)[2] has been attempted for the pursuit of trapping smaller nanoparticles. However, the heat generation accompanying the plasmonic excitation also causes thermal convection and thermophoresis.[3–7] The trapping in the vicinity of heat sinks has also been tried to overcome the temperature elevation,[8] but it is still difficult to sufficiently suppress the heating of trapping domain. Nanostructured semiconductor-assisted (NASSCA) trapping technique has recently been developed[9] as the non-plasmonic and non-thermal nanoparticle trapping. NASSCA trapping is advantageous for avoiding the heating up because of the high thermal conductivity (148 W/(K·m))[10] and low absorbance index index (950 cm^{-1}).[11] Therefore, the total grip force or stiffness of NASSCA optical tweezers turned out to be larger than plasmonic optical tweezers.[9] Namely, it is basically free from the

subtraction of the trapping force by the thermophoretic force. It is also favorable to induce nonlinear photonic processes such as multi-photon absorption, which makes it promising to induce photo-reaction while trapping the objects. In contrast, the window of laser intensity for stable trapping is narrowly limited for plasmonic optical trapping, because the repulsive force due to thermophoresis easily overcomes the optical trapping force.[4] Since the origin of electric field enhancement in NASSCA optical tweezers is multiple light scattering within the nano-needles on a solid (i.e., the so-called black Si) surface, it does not require the electronic excitation of the solid material itself. Therefore, a wide range of laser wavelength can be used for NASSCA trapping, which is called the broad-band optical manipulation. Furthermore, it is fairly easy (i.e., fast and low-cost) to fabricate the structure of black Si required by NASSCA as will be addressed in the next section, whereas the plasmonic structures are generally fabricated by rather low through-put and high-cost technique such as focused electron beam lithography.

NASSCA trapping also demonstrated one- and two-dimensional switchable trapping of multiple polystyrene nanoparticles, where the selection of specific structure is nontrivial.[12] This switching was realized by the spot size control of the laser irradiation. Therefore, the semiconductor-assisted approach has started attracting attention of the researchers.[13] The optical trapping of multiple nanoparticles can induce novel dynamics and collective structures.[14] In this article, the term "collective" is intended for characteristics that originates from the interaction of the discrete elements that constitute the system of interest. Trapping of many particles is also important in the applied situations such as the crystallization of colloidal particles for e.g., optical metamaterials[15] and organic molecules for e.g., X-ray analysis and pharmaceutics,[16,17] and the aggregation-induced emission (AIE).[18] In particular, the collective structural order formation in liquid with a reversible protocol is promising for the realization of reconfigurable photonic crystals in liquid. This is desired from the related technology where the optical fiber contains liquid components for functionality.

Furthermore, a recent report has theoretically proved the longer trapping duration is re-

alized by the loose trapping when the shape of force field is varied while the potential energy gap is the same.[19] In fact, the application of the simplest Arrhenius-type model for this problem is just an assumption, or the approximation for the convenience of calculation. The direct numerical analysis of the Langevin equation and analytical formulation revealed the significant difference of the actual dynamics from the useful approximation. Therefore, trapping many numbers of particles with special force field realized by the unconventional optical arrangements is of greater importance now. Here we report a large number of nanoparticles trapped in a domain formed by large area of laser irradiation with a regular packing structure with NASSCA trapping approach. Here, the term "regular" structure stands for a clear periodic one such as well-known crystals. It should be noted that the laser power is not higher than the previous report[9] where a single particle was trapped. The difference is in the use of multimodal laser, which cannot focus up to the level of diffraction limit and hence not used for single particle trapping.

Experimental details

NASSCA trapping is realized by the laser irradiation on the so-called black silicon (b-Si). The b-Si substrate was prepared by dry plasma etching (20 min.) in SF_6 and O_2 mixture[20] (cf. Fig. 1(a)). The detail of fabrication method and spectroscopic characterization of b-Si have been previously described.[9] The b-Si is a needle-like structure of silicon substrate as shown in the scanning electron microscope (SEM) image of Fig. 1(b). The height of the nanoneedles was ca. 200 nm on average and the diameter was 40 to 240 nm on surfaces.[9] The b-Si substrate was exposed to the sample solution of fluorescent polystyrene nanospheres with a diameter of 500 nm (Invitrogen, FluoSphreres F8813) and a concentration of 1.5×10^{-9} particles/mL. The experimental setup including the optical system is shown in Fig. 1(c). For NASSCA optical tweezers, a continuous-wave near-infrared (NIR) laser beam (wavelength 808 nm, Spectra-Physics, ProLite CW CWA0400-808-30-01) was loosely focused on the b-Si

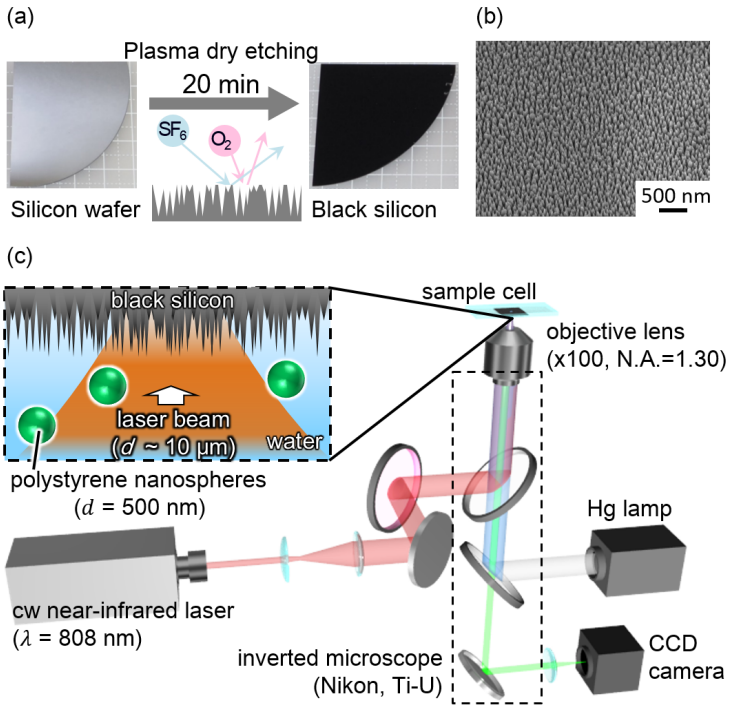

Figure 1: Experimental setup: (a) schematic diagram of the black Si (b-Si) fabrication, (b) Scanning electron microscopy (SEM) image of b-Si substrate, and (c) Schematic diagram of the measurement system.

surface with an objective lens (N.A. 1.30, magnification $\times 100$) of an inverted optical microscope (Nikon, Ti-U). In our previous study of NASSCA trapping,[9] the semiconductor laser has a laser beam quality closer to TEM_{00}. In contrast, we employed the multimodal laser usually oriented for material processing in this study. Considering the limitation of focusing level, the use of the industrial laser for trapping study is unusual. Our purpose is to realize a large area of irradiation with acceptable level of powers. The trapping behaviors were observed by fluorescence microscopy and recorded with a color charge-coupled-device (CCD) (frame rate of 117.6 fps, exposure time of ca. 8.3 ms, and resolution of 40 nm/px). We carried out NASSCA optical trapping by changing laser intensity at the same position for the examination of laser power dependence on the structure and dynamics of the nanoparticles. We extracted the particles trajectories from the obtained microscopy movie data. The algorithm is based on Ref.[21] First, the feature point detection for each image is

executed. Then, the identification of each detected feature points between the consecutive images. The radius of particles to be detected in the images and the intensity percentile for detection is necessary for the definition of particle in the images, and the identification of the same particles requires the limit of possible displacement. The input parameters for the tracking were as follows: Radius: 7 (px), Cutoff: 0, Intensity percentile: 20, Link range: 1, Displacement threshold: 7 (px). Once the trajectory data is obtained, we analyzed the characteristics of the dynamics.[14,22] Our analysis is based on the time-sequential images in two-dimensions without any distinction of the position in the direction perpendicular to the observation plane. In such cases when the particles had piled up on the b-Si, the outermost layers were observed and analyzed as they were the only observable part. The piling up had been qualitatively observed for different conditions of the experimental setup in our previous study.[9]

Results and discussion

Fig. 2(a) shows the snapshots of trapped nanoparticles in a steady state for different laser powers by fluorescence images. The higher power of laser irradiation tend to cause larger domain of particle assembly. Here, the term "assembly" simply means that a distinctive structure consisting of multiple particles formed from the original state without any structural order. The size of the trapping domain is in the order of 10 μm, which is huge considering the level of laser focusing and power. The number of trapped particles are much larger than the previous demonstration of NASSCA trapping experiment.[9] Furthermore, at sufficiently high laser power leads to the formation of regular packing of nanoparticles, whereas the particle assembly does not show a regular structure at lower laser powers. It should also be noted that this regular packing is realized by the subtle condition of the Si needle structure of the black Si. The same laser power does not necessarily leads to this level of regular packing when different locations in the same substrate were selected. The exact sufficient condition

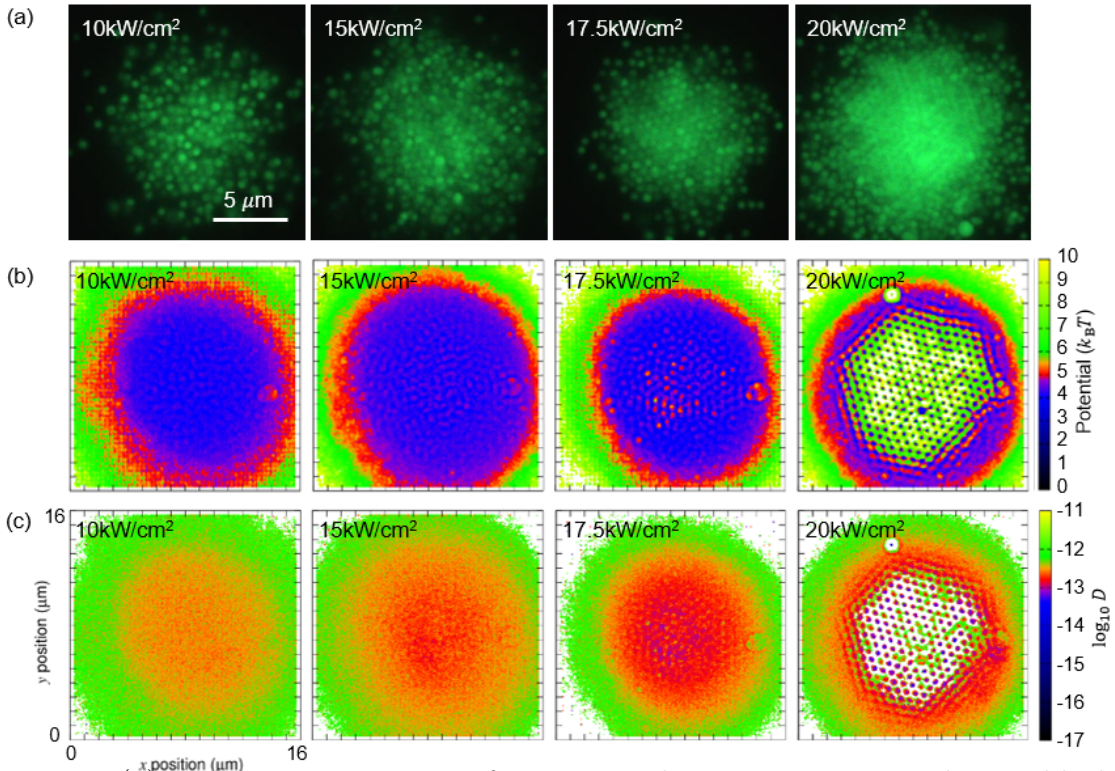

Figure 2: (a) Fluorescence images of 500-nm polystyrene nanoparticles on black silicon substrate subject to the laser irradiation, (b) two-dimensional maps of potential energy and (c) logarithm of diffusion coefficients for different laser powers after 30 min. from the start of the laser irradiation. The potential is evaluated based on Eq. 1. As with the potential in general, the relative difference within a map is the significant information, whereas the absolute value does not make much sense. The diffusion coefficient is based on the slope of mean squared displacement with a simplification as the normal diffusion for a time span of frame interval, i.e., 8.5×10^{-3} s.

of this needle structure specification is beyond the scope of this study. Nevertheless, this location dependence clearly indicates the essential role of the substrate in combination with the laser irradiation. In other words, the collective structure formation is not due to the inter-particle interactions that exist without laser nor b-Si. This regular collective structure was formed in tens of minutes after starting the laser irradiation. This process is shown in Fig. 3(a).

On condition that sufficient number density of particles exists in the observation domain and the system is at least in a steady state, the particle position distribution $p(\boldsymbol{r})$ can be evaluated and be transformed into the potential energy (or free energy) $\phi(\boldsymbol{r})$ of the laser

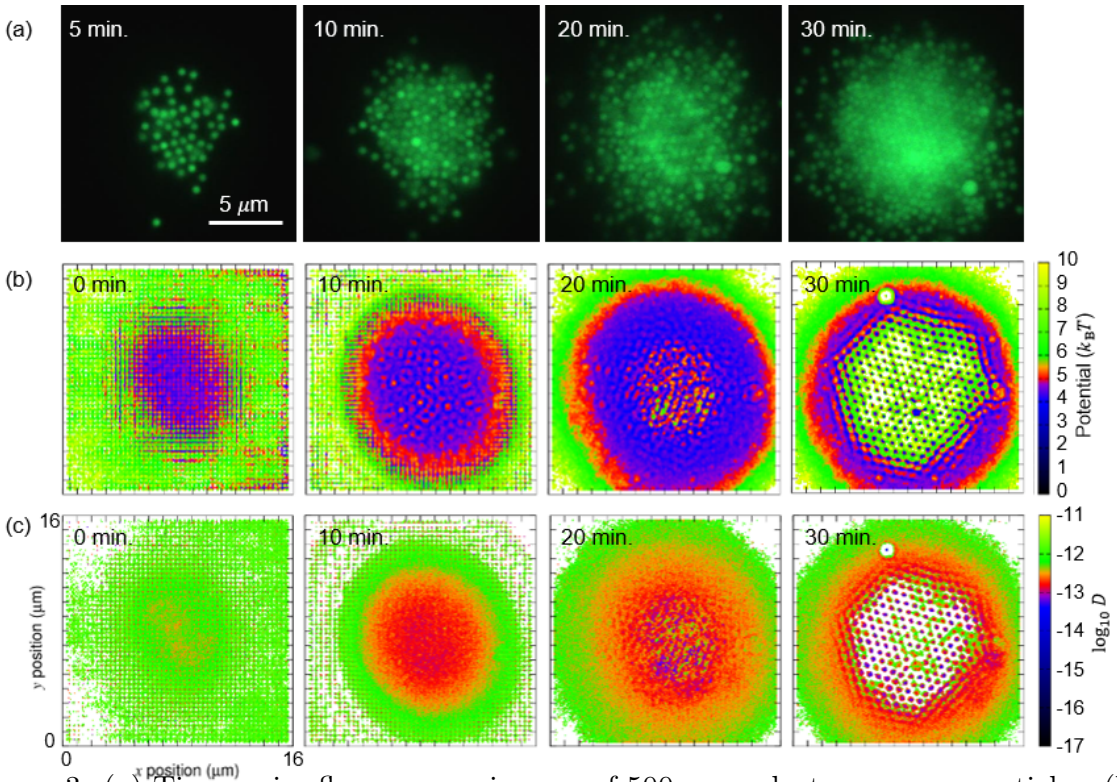

Figure 3: (a) Time-series fluorescence images of 500-nm polystyrene nanoparticles, (b) two-dimensional maps of potential energy and (c) logarithm of diffusion coefficients for the laser power of 20 kW/cm^2 in time series. The analysis for 0, 10, 20, 30 min. is conducted for the movies in the periods starting from each time point for 10^4 frames with 117.594 fps, which corresponds to 85 s of movie duration. The potential is evaluated based on Eq. 1. As with the potential in general, the relative difference within a map is the significant information, whereas the absolute value does not make much sense. The diffusion coefficient is based on the slope of mean squared displacement with a simplification as the normal diffusion for a time span of frame interval.

trapping:[19]

$$\phi(\boldsymbol{r}) = -k_{\mathrm{B}}T \ln p(\boldsymbol{r}), \tag{1}$$

where k_{B} and T are the Boltzmann constant and absolute temperature, respectively. Fig. 2(b) shows the potential energy map of the systems with different laser powers. It should be noted that the white (or blank) spots indicate that there had been no particles within the particle tracking period of time. By construction, Eq. 1 can be discussed only where the probability is larger than zero. Therefore, the undefined part corresponds to the higher potential compared to the determined highest potential in the map. Baring this in mind, the potential energy

difference between inside and outside of the trapping domain is understood as *at least* ca. 10 $k_{\mathrm{B}}T$. In spite of the fact that the laser irradiation was observed at the same location of the substrate, the potential energy landscape within the range from 10 kW/cm^2 to 17.5 kW/cm^2 is similar, and makes contrast with the 20 kW/cm^2 leading to the clearly regular packing. The clear point-wise distribution within the trapping domain implies that the potential energy landscape is not flat there but rather ragged. Otherwise, the symmetry of the system would cause the intermittent rotation of the assembled cluster at the solid-liquid interface.[14] The highly nonlinear relation between the laser power and trapping force field enhanced by the needle-like structure of the black Si can be observed as the strongly trapping spot with roughly single particle size at 20 kW/cm^2, which does not exist when the laser power was 17.5 kW/cm^2 or lower.

The zoomed-in figures of the central parts of particle assembly for different laser powers are shown in Fig. 4(a). In spite of the same location of black Si, the collective structure of the particles are different depending on the laser power. In particular, the regular packing structure at 20 kW/cm^2 was not observed when lower laser powers were applied to the system. The zoomed-in figure for 20 kW/cm^2 also reveals the slight anisotropy of the regular-packing that the trapped spots of respective nanoparticles are prolate in the similar orientation. The quantitative evaluation of the collective structures by radial distribution functions (RDF) is shown in Fig. 4(b) and (c). Although RDF does not distinguish the orientation of the structure, it reveals some characteristics unclear from the two dimensional maps. The nearest neighbors are located close to but in a slightly larger distance from that (i.e., 500 nm) of the contact state. The randomly-aligned inter-needle distances of b-Si are substantially smaller than the possible particle neighboring distance in two dimensions. Therefore, it is not the direct topography of b-Si but the optical force field generated by the combination of topography and the laser that constrain the location of nanoparticles in a specified regular packing. The collective structure beyond the scale of 3 μm is observed for 17.5 kW/cm^2, but the structural order extending to 10 μm is present only for 20 kW/cm^2 among the examined

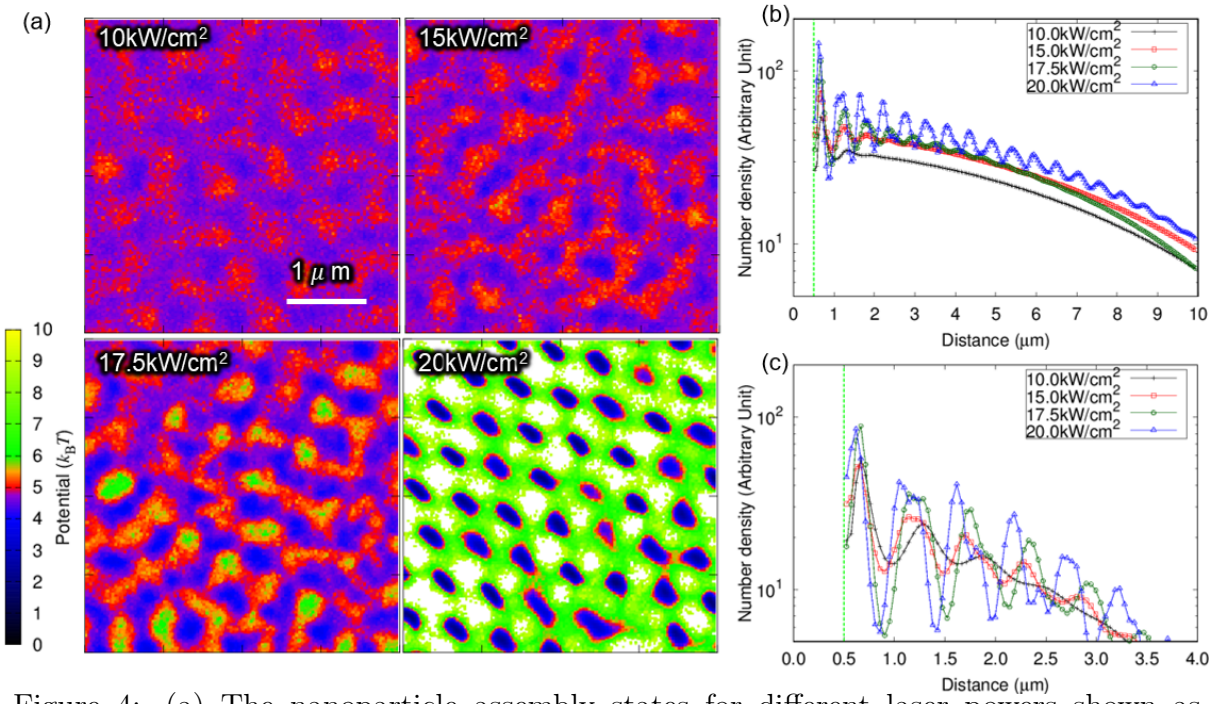

Figure 4: (a) The nanoparticle assembly states for different laser powers shown as the zoomed-in maps of potential energy, and (b),(c) radial distribution functions. The potential is evaluated based on Eq. 1. As with the potential in general, the relative difference within a map is the significant information, whereas the absolute value does not make much sense. The sampled domain size for (b) and (c) corresponds to Figs. 2 and 4(a), respectively. The samples of projected distances are collected from 500 nm as the particle diameter is 500 nm and overlapping are not taken into account in the microscopy images.

four conditions. The location of peaks are also different for different laser powers.

Since the potential energy landscape is simply derived from the position distribution of the particles without time dependence, the dynamics is another story. The particle tracking analysis includes the information of the dynamics. The stochastic dynamics is evaluated as the diffusion coefficient. Fig. 2(c) shows the highly inhomogeneous distribution of diffusion coefficients. Because of the large range of diffusion coefficients to be mapped in a single figure, the logarithm is mapped.[14,23,24] The bulk diffusion coefficient of 500-nm-sized nanoparticles in water is ca. 10^{-12} m^2/s based on the Stokes-Einstein relation. The trapped nanoparticles at the peripheral part of the trapping domain exhibit this bulk value of the diffusion coefficient. The higher laser power leads to smaller diffusion coefficients in the central part of the trapping domain. The regularly-packed nanoparticles exhibits smallest diffusion coefficients

in the domain, and the occasional translocation from a trapping site to another one takes place with a larger diffusion coefficient similar to the bulk value. In general, the extremely high concentration[25] and vicinity to a solid wall are the suppressing factor of the diffusion coefficient by hydrodynamic effects.[26–32] However, the needle-like topography of the black Si is nontrivial to estimate this wall effect. On the other hand, the irradiation of laser causes scattering force as well as the gradient force. This non-conservative force can drive incessant stochastic motion.[14] The one or two orders of smaller diffusion coefficient compared to the bulk value suggests the dominant conservative force on the nanoparticles at the time scale of frame intervals.

As already shown by the fluorescence images in Fig. 3, the collective structure was formed in tens of minutes. Assuming that the 10^4 frames corresponding to ca. 85 s are approximately regarded as steady state, the corresponding potential energy landscape and diffusion coefficient field are shown as time series in Fig. 3(b) and (c). There is a fundamental limitation that the particle concentration is too small to conclude the early stage of smaller number of particles are caused by smaller trapping domain (e.g., the fluorescence image at 5 min. of Fig. 3(a)). Nevertheless, there is a feature in the transient period of collective structure formation. The central part of the trapping domain once shows slightly higher potential energy than the surrounding part at around 20 min. This is understood as the characteristics of metastable structure before being regularly packed. The metastable structure was temporarily maintained with potential energy differences or a few $k_{\mathrm{B}}T$. Then, the converged regular structure shows the potential energy differences at least several times larger than those of the metastable structure. The diffusion coefficient is substantially smaller than that in a bulk state once the sufficient nanoparticle concentration is attained at the central part. Then, the subdomain of this small diffusion coefficient extends the size. It appears that the regularly-packed state is realized when the size of trapping domain stops to grow. The transient period of particle assembly does not show the regular packing structure. The regular packing requires the sufficiently high local concentration of the nanoparticles, but it is not a

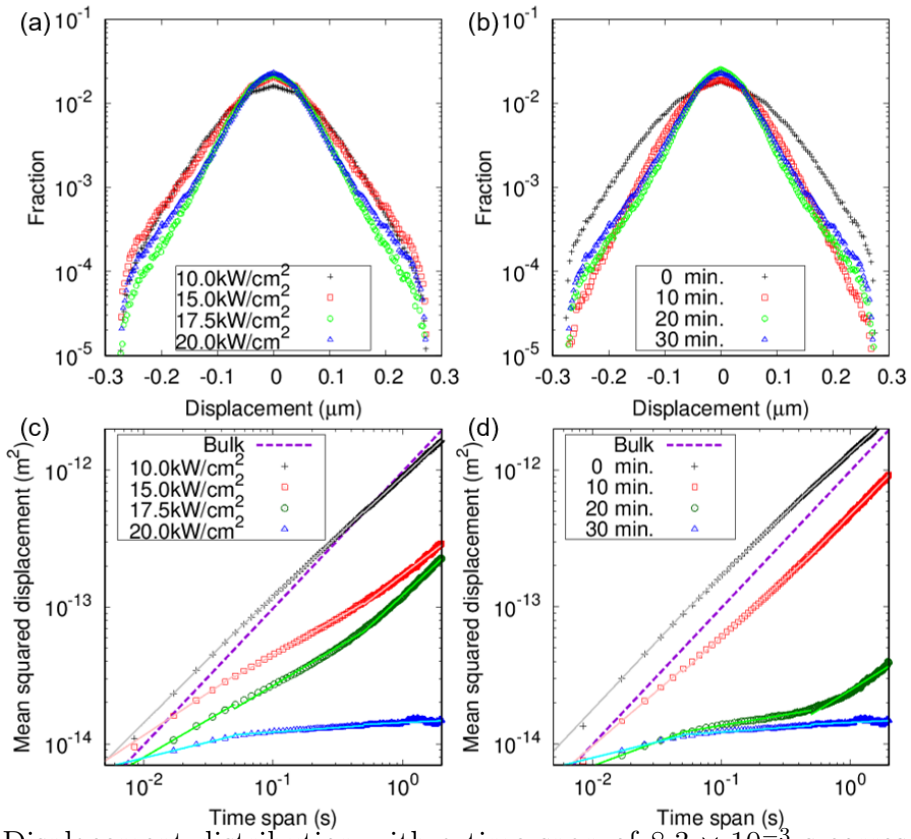

Figure 5: Displacement distribution with a time span of 8.3×10^{-3} s corresponding to the frame rate of 120 fps for (a) different laser powers and in (b) time series, and mean squared displacements (MSDs) as a function of time for (c) different laser powers in a steady state and (d) in time series at 20 kW/cm^2. The size of the sampled domain corresponds to Fig. 4(a). The dashed line of the bulk value is derived from the Stokes-Einstein relation.

sufficient condition.

As suggested in Fig. 2(c) for the case of 20 kW/cm^2, the stochastic dynamics of nanoparticles in the central subdomain is likely to be different from the simplest form of Brownian motion. Since the dynamics is highly non-uniform depending on the distance from the laser focus, we examine the displacement distribution at frame intervals in the central subdomain of the system (e.g., Fig. 4(a)) as shown in Figs. 5 (a) and (b). The higher laser power leads to more highly non-Gaussian distribution of the displacements, where the probability is more concentrated into the smaller displacements. The higher probabilities for larger displacements at 20 kW/cm^2 compared to those at 17.5 kW/cm^2 is considered to be the difference of collective structure. The occasional jumps from one stable trapping site from another

is faster when it happens because of the conservative force acting on the nanoparticles, compared to the incessant dynamics at the less localized trapping state. The nanoparticles show the displacement distribution closer to the Gaussian one at the stage of increasing concentration, compared to that at the later stage after the concentration saturated. The sufficiently crowded state of nanoparticles, where the nanoparticles interact with each other in the trapping domain, leads to the non-Gaussian displacement distributions.

The displacement distribution and time evolution of mean squared displacements (MSDs) are different aspects of stochastic dynamics.[33] The diffusion coefficients mapped in Figs. 2(c) and 3(c) are based on an assumption of normal diffusion where the MSD is a linear function of time. However, the trapped state indicates the nonlinearity of the dynamics. Fig. 5(c) shows that the slope of the MSD is smaller but the MSD itself is slightly yet significantly larger within a second of the time span at 10 kW/cm^2, compared to the bulk normal diffusion derived from the Stokes-Einstein relation. This means that the dynamics at 10 kW/cm^2 is already subdiffusive, *i.e.*, the slope of the time derivative of MSD decreases with time, within the time scale of a few seconds, but the stochastic motion is enhanced presumably by the non-conservative optical force. As the laser power is increased, the MSD for a specific time span decreases. The slope of the MSD also decreases with the increase of the laser power, but the scaling of the MSD as a function of time also changes with the range of time scale. The time evolution of the nanoparticle assembly shown in Figs. 5(d) indicates that the initial stage of increasing concentration exhibits more enhanced stochastic motion than the bulk normal diffusion. Then, the dynamics becomes gradually subdiffusive. The curve at 20 min. compared to that at 30 min. suggests that the slow down of the stochastic dynamics at shorter time span (< 1 s) proceeds earlier than that at the larger time span (≥ 1 s).

Conclusions

Combination of NASSCA optical trapping with multimodal industrial laser source leads to the large area of nanoparticle trapping domain with standard laser powers. When trying to collect as many particles as possible rather than fixing the position of a single particle, the focusing sharpness is not of primary importance. With an aid of needle-like topography of b-Si, the stable trapping of large amount of nanoparticles were realized. Furthermore, the fine combination of b-Si structure with 20 kW/cm^2 results in a regularly-packed collective structure of the nanoparticles. Considering the randomness and narrower spacing of Si needles compared to the nanoparticle size and symmetry of the laser irradiation, this regularly packed state is caused by a nontrivial interplay of the laser and substrate. These findings are important in the applications ranging from optical metamaterial formation to the aggregation-induced emission. Furthermore, it is of particular importance in the realization of reconfigurable photonic crystals in liquid. Trapping large collection of nanoparticles and tight tweezing of a single particle require distinctive approaches while they are directly related with each other.

Acknowledgement

The authors acknowledge Prof. Saulius Juodkazis (Swinburne University, Melbourne, Australia) for providing us with the black Si substrate. This work was partly supported by JSPS KAKENHI Grant Numbers 17H05463, JP17K04974, JP18K14254, JP16H06504/ JP16H06506/ JP16H06507 in Scientific Research on Innovative Areas "Nano-Material Manipulation and Structural Order Control with Optical Forces" and "Molecular Engine" (JP19H05402).

Supporting Information Available

- 10kWcm2.mp4: The compressed movie data at the laser power density of 10kW/cm^2.

- 15kWcm2.mp4: The compressed movie data at the laser power density of 15kW/cm^2.
- 17.5kWcm2.mp4: The compressed movie data at the laser power density of 17.5kW/cm^2.
- 20kWcm2.mp4: The compressed movie data at the laser power density of 20kW/cm^2.

References

(1) Ashkin, A.; Dziedzic, J. M.; Bjorkholm, J. E.; Chu, S. Observation of a Single-beam Gradient Force Optical Trap for Dielectric Particles. *Opt. Lett.* **1986**, *11*, 288.

(2) Shoji, T.; Tsuboi, Y. Plasmonic Optical Tweezers toward Molecular Manipulation: Tailoring Plasmonic Nanostructure, Light Source, and Resonant Trapping. *J. Phys. Chem. Lett.* **2014**, *5*, 2957–2967.

(3) Roxworthy, B. J.; Ko, K. D.; Kumar, A.; Fung, K. H.; Chow, E. K. C.; Liu, G. L.; Fang, N.; Toussaint, K. C. Application of Plasmonic Bowtie Nanoantenna Arrays for Optical Trapping, Stacking, and Sorting. *Nano Lett.* **2012**, *12*, 796–801.

(4) Shoji, T.; Saitoh, J.; Kitamura, N.; Nagasawa, F.; Murakoshi, K.; Yamauchi, H.; Ito, S.; Miyasaka, H.; Ishihara, H.; Tsuboi, Y. Permanent Fixing or Reversible Trapping and Release of DNA Micropatterns on a Gold Nanostructure Using Continuous-Wave or Femtosecond-Pulsed Near-Infrared Laser Light. *J. Am. Chem. Soc.* **2013**, *135*, 6643–6648.

(5) Gargiulo, J.; Brick, T.; Violi, I. L.; Herrera, F. C.; Shibanuma, T.; Albella, P.; Requejo, F. G.; Cortés, E.; Maier, S. A.; Stefani, F. D. Understanding and Reducing Photothermal Forces for the Fabrication of Au Nanoparticle Dimers by Optical Printing. *Nano Lett.* **2017**, *17*, 5747–5755.

(6) Pin, C.; Ishida, S.; Takahashi, G.; Sudo, K.; Fukaminato, T.; Sasaki, K. Trapping and

Deposition of Dye-Molecule Nanoparticles in the Nanogap of a Plasmonic Antenna. *ACS Omega* **2018**, *3*, 4878–4883.

(7) Jiang, Q.; Rogez, B.; Claude, J.-B.; Baffou, G.; Wenger, J. Temperature Measurement in Plasmonic Nanoapertures Used for Optical Trapping. *ACS Photonics* **2019**, *6*, 1763–1773.

(8) Wang, K.; Schonbrun, E.; Steinvurzel, P.; Crozier, K. B. Trapping and Rotating Nanoparticles Using a Plasmonic Nano-tweezer with an Integrated Heat Sink. *Nat. Commun.* **2011**, *2*, 469.

(9) Shoji, T.; Mototsuji, A.; Balcytis, A.; Linklater, D.; Juodkazis, S.; Tsuboi, Y. Optical Tweezing and Binding at High Irradiation Powers on Black-Si. *Sci. Rep.* **2017**, *7*, 12298.

(10) Lide, D. R. *CRC Handbook of Chemistry and Physics*; CRC Press Taylor & Francis, 2014.

(11) Aspnes, D. E.; Studna, A. A. Dielectric Functions and Optical Parameters of Si, Ge, GaP, GaAs, GaSb, InP, InAs, and InSb from 1.5 to 6.0 eV. *Phys. Rev. B* **1983**, *27*, 985.

(12) Roy, D.; Mondal, D.; Goswami, D. Structure and Dynamics of Optically Directed Self-assembly of Nanoparticles. *Sci. Rep.* **2016**, *6*, 23318.

(13) Xu, Z.; Crozier, K. B. All-dielectric Nanotweezers for Trapping and Observation of a Single Quantum Dot. *Opt. Exp.* **2019**, *27*, 4034.

(14) Hanasaki, I.; Hosokawa, C. Non-uniform Stochastic Dynamics of Nanoparticle Clusters at a Solid-liquid Interface Induced by Laser Trapping. *Jpn. J. Appl. Phys.* **2019**, *58*, SDDK07.

(15) Gwo, S.; Chen, H.-Y.; Lin, M.-H.; Sun, L.; Li, X. Nanomanipulation and Controlled

Self-assembly of Metal Nanoparticles and Nanocrystals for Plasmonics. *Chem. Soc. Rev.* **2016**, *45*, 5672–5716.

(16) Rocca, J. D.; Liu, D.; Lin, W. Nanoscale Metal-organic Frameworks for Biomedical Imaging and Drug Delivery. *Acc. Chem. Res.* **2011**, *44*, 957–968.

(17) Tschierske, C. Development of Structural Complexity by Liquid-Crystal Self-assembly. *Angew. Chem. Int. Ed.* **2013**, *52*, 8828–8878.

(18) Hong, Y.; Lam, J. W. Y.; Tang, B. Z. Aggregation-induced Emission: Phenomenon, Mechanism and Applications. *Chem. Commun.* **2009**, 4332–4353.

(19) Hanasaki, I.; Nemoto, T.; Tanaka, Y. Soft Trapping Lasts Longer: Dwell Time of a Brownian Particle Varied by Potential Shape. *Phys. Rev. E* **2019**, *99*, 022119.

(20) Ivanova, E. P.; Hasan, J.; Webb, H. K.; Gervinskas, G.; Juodkazis, S.; Truong, V. K.; Wu, A. H. F.; Lamb, R. N.; Baulin, V. A.; Watson, G. S.; Watson, J. A.; Mainwaring, D. E.; Crawford, R. J. Bactericidal Activity of Black Silicon. *Nat. Commun.* **2013**, *4*, 2838.

(21) Sbalzarini, I. F.; Koumoutsakos, P. Feature Point Tracking and Trajectory Analysis for Video Imaging in Cell Biology. *J. Struct. Biol.* **2005**, *151*, 182–195.

(22) Motohashi, R.; Hanasaki, I. Characterization of Aqueous Cellulose Nanofiber Dispersions from Microscopy Movie Data of Brownian Particles by Trajectory Analyss. *Nanoscale Advances* **2019**, *1*, 421–429.

(23) Hanasaki, I.; Uehara, S.; Arai, Y.; Nagai, T.; Kawano, S. Threshold-free Evaluation of Near-surface Diffusion and Adsorption-dominated Motion from Single-molecule Tracking Data of Single-stranded DNA through Total Internal Reflection Fluorescence Microscopy. *Jpn. J. Appl. Phys.* **2015**, *54*, 125601.

(24) Motohashi, R.; Hanasaki, I.; Ooi, Y.; Matsuda, Y. Robust Evaluation of Diffusion Coefficient against Displacement Threshold Parameter of Single Particle Tracking Algorithm. *Micro Nano Lett.* **2017**, *12*, 506–510.

(25) Happel, J.; Brenner, H. *Low Reynolds Number Hydrodynamics*; Kluwer Academic Publishers Group, 1983.

(26) Faxén, H. Der Widerstand Gegen die Bewegung einer Starren Kugel in einer zähen Flüssigkeit, die Zwischen Zwei Parallelen Ebenen Wäanden Eingeschlossen ist. *Ann. Phys.* **1922**, *373*, 89–119.

(27) Brenner, H. The Slow Motion of a Sphere through a Viscous Fluid towards a Plane Surface. *Chem. Eng. Sci.* **1961**, *16*, 242–251.

(28) Goldman, A. J.; Cox, R. G.; Brenner, H. Slow Viscous Motion of a Sphere Parallel to a Plane Wall-I Motion through a Quiescent Fluid. *Chem. Eng. Sci.* **1967**, *22*, 637–651.

(29) Huang, P.; Breuer, K. S. Direct Measurement of Anisotropic Near-wall Hindered Diffusion using Total Internal Reflection Vlocimetry. *Phys. Rev. E* **2007**, *76*, 046307.

(30) Carvajal-Tinoco, M. D.; Lopez-Fernandez, R.; Arauz-Lara, J. L. Asymmetry in Colloidal Diffusion near a Rigid Wall. *Phys. Rev. Lett.* **2007**, *99*, 138303.

(31) Choi, C. K.; Margraves, C. H.; Kihm, K. D. Examination of Near-wall Hindered Brownian Diffusion of Nanoparticles: Experimental Comparison to Theories by Brennner (1961) and Goldman *et al.* (1967). *Phys. Fluids* **2007**, *19*, 103305.

(32) Holmqvist, P.; Dhont, J. K. G.; Lang, P. R. Colloidal Dynamics near a Wall Studied by Evanescent Wave Light Scattering: Experimental and Theoretical Improvements and Methodological Limitations. *J. Chem. Phys.* **2007**, *126*, 044707.

(33) Hanasaki, I.; Uehara, S.; Kawano, S. Role of Time Scales for the Non-Gaussianity of

the Brownian Motion Combined with Intermittent Adsorption. *J. Comp. Sci.* **2015**, *10*, 311–316.